Achromatic critically coupled racetrack resonators

Clément Arlotti, Olivier Gauthier-Lafaye, Antoine Monmayrant, Stéphane Calvez

Achromatic critically-coupled racetrack resonators

CLEMENT ARLOTTI,[1,*] OLIVIER GAUTHIER-LAFAYE,[1] ANTOINE MONMAYRANT,[1] STEPHANE CALVEZ[1]

[1]*LAAS, Univ de Toulouse, CNRS, 7 avenue du colonel Roche, F-31031 Toulouse, FRANCE*
**Corresponding author: carlotti@laas.fr*

Received XX Month XXXX; revised XX Month, XXXX; accepted XX Month XXXX; posted XX Month XXXX (Doc. ID XXXXX); published XX Month XXXX

In this paper, we investigate the spectral response of whispering-gallery-mode (WGM) resonators coupled to their access waveguide with a view to design their constitutive waveguides to promote critical-coupling over a wide spectral range and thereby facilitate their use for high-sensitivity sensing or nonlinear frequency conversion applications. The carried-out theoretical analysis is based on the universal response functions of singlemode and unidirectional devices. A coupled-mode treatment of the coupling region enables to derive two sets of favorable designs. The identified resonator/access waveguide systems exploit waveguides with mismatched propagation constants forming a coupling section exhibiting either an achromatic beat-length or an achromatic power-transfer coefficient. This generic model is followed by a numerical case study of vertically-coupled Si_3N_4 racetrack resonators. The conventional (quasi-)phase-matched configuration, treated as a reference case, is shown to display a critical-coupling bandwidth of 23 nm at a wavelength of 1550nm, whereas the proposed new designs demonstrate critical bandwidths larger than 330nm, i.e. exhibit bandwidths enhanced by more than one order of magnitude.

OCIS codes: *(130.3120) Integrated optics devices; (230.4555) Coupled resonators; (130.3990) Micro-optical devices; (230.5750) Resonators; (230.7370) Waveguides.*

http://dx.doi.org/10.1364/AO.99.099999

1. INTRODUCTION

Over the last decades, integrated whispering-gallery-mode (WGM) resonators have been increasingly used as the basic building blocks for photonics components [1] since they can provide high-quality factors and large field enhancement. For instance, recent developments in integrated non-linear optics have demonstrated that parametric cascaded four-wave mixing in high-Q Si_3N_4 micro-resonators is an effective approach for optical frequency comb generation [2]. Silicon-based micro-resonators have also emerged as a new technology for highly sensitive detection of analytes in liquid or gas, based on optical resonance shift tracking [3][4]. In any case, the performance of these WGM resonators is governed by the round-trip propagation loss in the resonator section, whose contribution is aimed to be as small as possible, and by the evanescent coupling of the light between the constitutive cavity and access waveguide(s). For devices with transversely singlemode resonator and access waveguides, the system is said to be critically coupled when the in-coupling rate balances the round-trip loss. In this situation, the intracavity power is maximum [5] and the transfer function of the system drops to zero due perfectly destructive interference between the input waveguide incident field and the outcoupled resonator field [6], thereby maximizing the response contrast of the system. A direct consequence of these two properties is that, in the aforementioned applications, there is an incentive to achieve this critical coupling condition over a large spectral range to promote nonlinear interactions or to enhance the sensor detection capabilities. Chandran *et al* have done so by implementing symmetric couplers with long coupler interaction length [7].

In this article, we theoretically derive two sets of favorable coupling conditions to obtain achromatic critically-coupled racetrack resonators using asymmetric coupling regions. The benefits of the proposed designs in terms of critical coupling bandwidth enhancement with respect to the more conventional (quasi-)phase-matched approach are subsequently illustrated through the numerical investigation of the spectral response of racetrack resonators made of Si_3N_4/SiO_2 and whose evanescent coupling takes place vertically between the rounded-rectangle resonator and its underlying access waveguide (see Fig. 1.).

2. THEORETICAL MODEL

The theoretical analysis carried out here is based on the universal description of the system characteristics [6] with a complete Coupled-Mode Theory (CMT) treatment of the evanescent coupling section of length L [8] (see Fig. 1. and Fig. 3(a)).

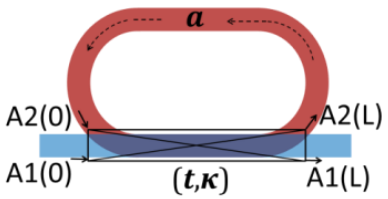

Fig. 1. Schematic of the studied vertically-coupled racetrack resonator.

The resonator intracavity power P_{int} (resp. intensity transmission T) consists of a set of Lorentzian peaks (resp. dips) separated by the resonator free spectral range and modulated by an upper (resp. lower) envelop given, at the resonance wavelength, λ, by [6]:

$$P_{int}(\lambda) = \left|\frac{A_2(L)}{A_1(0)}\right|^2 = \frac{a(\lambda)^2(1-|t(\lambda)|^2)}{(1-a(\lambda)|t(\lambda)|)^2}\, P_i(\lambda) \quad (1)$$

$$T(\lambda) = \left|\frac{A_1(L)}{A_1(0)}\right|^2 = \frac{(a(\lambda)-|t(\lambda)|)^2}{(1-a(\lambda)|t(\lambda)|)^2} \quad (2)$$

where $t(\lambda)$ is the amplitude transmission coefficient of the codirectional coupler, $a(\lambda)$ is the single-pass transmission coefficient of the resonator and $P_i(\lambda)$ is the spectral density at the input of the system.

For a resonator of total length, L_R, with an averaged intensity loss propagation constant, ρ, the latter parameter is given by:

$$a(\lambda) = e^{-\frac{\rho(\lambda)}{2}L_R} \quad (3)$$

Simulating the coupling section as a coupler constituted of two parallel waveguides (of length L), the CMT expression of t is given as follows [8] :

$$t(\lambda, L) = \cos(\Gamma(\lambda)L) + j\frac{\widehat{\delta(\lambda)}}{\Gamma(\lambda)}\sin(\Gamma(\lambda)L) \quad (4)$$

where

$$\Gamma(\lambda) = \sqrt{\kappa_a(\lambda)\kappa_b(\lambda) + \widehat{\delta(\lambda)}^2} \quad (5)$$

is the wavevector of the power transfer oscillations. κ_a, κ_b are the complete-CMT mode-overlap integrals calculated from the single transverse mode distributions of the constitutive access and resonator waveguides, and $\widehat{\delta(\lambda)}$ represents the complete-CMT effective propagation constant mismatch

$$\widehat{\delta(\lambda)} = \frac{\beta_{wg}(\lambda)-\beta_R(\lambda)}{2} + \frac{\alpha_a-\alpha_b}{2} \quad (6)$$

where α_a and α_b are the complete-CMT self-coupling coefficients, i.e corrections induced by the coupling interaction to the propagation constants of the isolated waveguides. As mentioned above, maximizing the intra-cavity power using (1) (or equivalently minimizing the system transmission using (2)), leads to the critical coupling condition:

$$a(\lambda) = |t(\lambda)| \quad (7)$$

Expanding the square modulus of the latter relationship and using equations (4) to (6) leads to

$$a(\lambda)^2 = 1 - F(\lambda)sin^2(\pi L/L_\pi(\lambda)) \quad (8)$$

where $L_\pi(\lambda)$ and $F(\lambda)$ represent respectively the coupler characteristic beat length and power-coupling efficiency as illustrated in Fig. 2 for a fixed wavelength and different coupler designs. The expressions for these parameters are respectively:

$$L_\pi(\lambda) = \pi/\Gamma(\lambda) \quad (9)$$

$$F(\lambda) = 1 - \left(\widehat{\delta(\lambda)}L_\pi(\lambda)/\pi\right)^2 \quad (10)$$

From the above (equations (5),(6) and (9)), it can be inferred that, at a set wavelength, as the phase mismatch increases, both F and L_π decrease. As a result and as shown in Fig. 2, the $|t(L)|^2$ spatial oscillation will progressively evolve from the red (phase matched) to the blue and green curves.

Using $f(\lambda) = a(\lambda)^2 - |t(\lambda)|^2$ as merit function, achieving broadband critical coupling corresponds to setting

$$f(\lambda) = 0\,, \forall\lambda \quad (11)$$

Although this might be computer intensive, this problem could be solved using a fully numerical optimization procedure allowing the routine to vary the waveguide cross-sections, separation, lateral offset and coupler length. To gain some physical insight, we have chosen to continue the theoretical treatment slightly further. In particular, the relevant solutions will verify, at a given wavelength, λ_0, the less restrictive set of conditions provided hereafter:

$$\begin{cases} f(\lambda_0) = 0 & (12a) \\ \left.\dfrac{\partial f(\lambda)}{\partial\lambda}\right|_{\lambda=\lambda_0} = 0 & (12b) \end{cases}$$

Equation (12a) represents the critical coupling condition while (12b) enforces the achromatic behaviour. Expanding equation (12a) means that the coupler length is restricted to a specific set of critical coupling lengths, $L_{cc}(\lambda, m^{\pm})$ ($m \in \mathbb{N}$), whose expression is:

$$L_{cc}(\lambda_0, m^{\pm}) = (x_{0\pm} + m)L_\pi(\lambda_0) \quad (13)$$

where $x_{0\pm}(\lambda_0)$ is the relative deviation from $L_\pi(\lambda_0)$ given by

$$x_{0\pm}(\lambda_0) = \frac{1}{\pi}arcsin\left(\pm\sqrt{(1-a(\lambda_0)^2)/F(\lambda_0)}\right) \quad (14)$$

Fig. 2 illustrates the fact that the system is critically coupled for coupler lengths such that the $|t(L)|^2$ spatial oscillation (red, blue or green depending of the considered phase-mismatch) curve intercepts the intensity inner circulation factor $a^2(L)$ (black line - which, as detailed in section 3.B, can be made independent of the coupler length). The meaning of equations (13)-(14) can thus clearly be understood : the critical coupling lengths are periodically found at a discrete set of values, symmetrically positioned around integer multiples (order m) of L_π. These critical coupling points are marked, in the phase-mismatched case, as the blue crosses occurring at each intersection between the $|t(L)|^2$ (blue) curve and the $a^2(L)$ (black) curve.

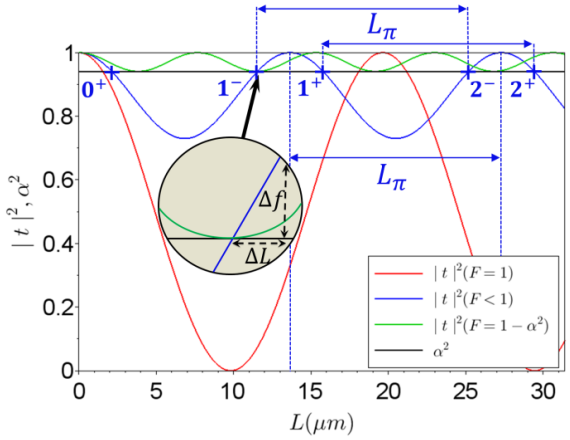

Fig. 2. Illustration of the coupler-only power transmission characteristics taken at the access-waveguide output port as a function of the coupler length and for couplers whose access and resonator waveguides exhibit identical (phase-matched, F=1) or different (phase-mismatched, F<1) propagation constants. The critical coupling lengths and L_π are highlighted in blue, for a phase mismatched case. Inset: Zoom-in view of L_π-coupling sensitivity for the two proposed achromatic critical-coupling scenarii.

Noting that a, $\hat{\delta}^2$ and $K(\lambda)=\kappa_a(\lambda)\kappa_b(\lambda)$ are independent variables, expanding equation (12b) leads to:

$$\left.\frac{\partial f(\lambda)}{\partial \lambda}\right|_{\lambda=\lambda_0} = 2a(\lambda)\left.\frac{\partial a(\lambda)}{\partial \lambda}\right|_{\lambda=\lambda_0} + \left.\frac{\partial f(\lambda)}{\partial K}\right|_{K=K(\lambda_0)} \left.\frac{\partial K(\lambda)}{\partial \lambda}\right|_{\lambda=\lambda_0} + \left.\frac{\partial f(\lambda)}{\partial \hat{\delta}^2}\right|_{\hat{\delta}^2=\widehat{\delta(\lambda_0)}^2} \left.\frac{\partial \hat{\delta}^2(\lambda)}{\partial \lambda}\right|_{\lambda=\lambda_0} = 0 \quad (15)$$

With

$$\left.\frac{\partial f(\lambda)}{\partial K}\right|_{K=K(\lambda_0)} = \frac{L_\pi(\lambda_0)^2}{2\pi^2}\sin\left(\frac{\pi L}{L_\pi(\lambda_0)}\right)\left[2(F(\lambda_0)-1)\sin\left(\frac{\pi L}{L_\pi(\lambda_0)}\right) - \frac{2\pi L F(\lambda_0)}{L_\pi(\lambda_0)}\cos\left(\frac{\pi L}{L_\pi(\lambda_0)}\right)\right] \quad (16)$$

and

$$\left.\frac{\partial f(\lambda)}{\partial \hat{\delta}^2}\right|_{\hat{\delta}^2=\widehat{\delta(\lambda_0)}^2} = \left.\frac{\partial f(\lambda)}{\partial K}\right|_{K=K(\lambda_0)} + \frac{L_\pi(\lambda_0)^2}{\pi^2}\sin^2\left(\frac{\pi L}{L_\pi(\lambda_0)}\right) \quad (17)$$

Assuming that the resonator losses are wavelength-independent, the achromatic critically-coupled designs are solutions of (13) and of the simplified equation:

$$\left.\frac{\partial f(\lambda)}{\partial K}\right|_{K=K(\lambda_0)} \left.\frac{\partial K(\lambda)}{\partial \lambda}\right|_{\lambda=\lambda_0} = -\left.\frac{\partial f(\lambda)}{\partial \hat{\delta}^2}\right|_{\hat{\delta}^2=\widehat{\delta(\lambda_0)}^2} \left.\frac{\partial \widehat{\delta(\lambda)}^2}{\partial \lambda}\right|_{\lambda=\lambda_0} \quad (18)$$

Two specific cases can then be considered. The first scenario corresponds to the case where the coupler length is such that it is close to $mL_\pi(\lambda_0)$ (i.e. x_0 is small). In this case, using a first order Taylor expansion, it can be shown that

$$\left.\frac{\partial f(\lambda)}{\partial \hat{\delta}^2}\right|_{\hat{\delta}^2=\widehat{\delta(\lambda_0)}^2} \sim \left.\frac{\partial f(\lambda)}{\partial K}\right|_{K=K(\lambda_0)} \sim x_0 L_\pi(\lambda_0) L F(\lambda_0) \quad (19)$$

Additionally, taking the wavelength-derivative of equation (9) (and using (5)) leads to:

$$\left.\frac{\partial L_\pi(\lambda)}{\partial \lambda}\right|_{\lambda=\lambda_0} = -\frac{L_\pi(\lambda_0)^3}{2\pi^2}\left(\left.\frac{\partial K}{\partial \lambda}\right|_{\lambda=\lambda_0} + \left.\frac{\partial \widehat{\delta(\lambda)}^2}{\partial \lambda}\right|_{\lambda=\lambda_0}\right) \quad (20)$$

Combining the last three equations reveals that

$$\left.\frac{\partial L_\pi(\lambda)}{\partial \lambda}\right|_{\lambda=\lambda_0} = 0 \quad (21)$$

This means that, in this situation, the evolution of the resonator and access waveguide optical confinement is compensated by the change in the mismatch between their propagation constants, i.e. the two spectral contributions of Equation (5) ($\kappa_a(\lambda)\kappa_b(\lambda)$ and $\widehat{\delta(\lambda)}^2$) compensate each other. This achromatic critically-coupled design thus corresponds to a system whose coupler beat length is achromatic.

A second scenario of interest is such that the coupler length is close to $(2m\pm1)L_\pi(\lambda_0)/2$ (i.e. $|x_0| \sim 0.5$). According to Equations (8) and (12a), in this situation (shown in green on Fig. 2), the coupler power–coupling efficiency, $F(\lambda_0)$, is close to the cut-off point where the minimum of the $|t(L)|^2$ spatial oscillations is tangent to $a(\lambda_0)^2$, i.e. $1-F(\lambda_0)\sim a^2(\lambda_0)$. It should be stressed that this entails that the system constitutive resonator and access waveguides have to exhibit mismatched effective propagation constants (to have F<1) i.e. to be phase mismatched (PMM). Equations (16) and (17) can then be approximated by:

$$\left.\frac{\partial f(\lambda)}{\partial K}\right|_{K=K(\lambda_0)} \sim \frac{L_\pi(\lambda_0)^2(F(\lambda_0)-1)}{\pi^2} \quad (22)$$

and

$$\left.\frac{\partial f(\lambda)}{\partial \hat{\delta}^2}\right|_{\hat{\delta}^2=\widehat{\delta(\lambda_0)}^2} \sim \frac{L_\pi(\lambda_0)^2 F(\lambda_0)}{\pi^2} \quad (23)$$

Furthermore, taking the wavelength-derivative of the power-coupling efficiency (equation (10)) leads to :

$$\left.\frac{\partial F(\lambda)}{\partial \lambda}\right|_{\lambda=\lambda_0} = \frac{L_\pi(\lambda_0)^2}{\pi^2}\left[(1-F)\left.\frac{\partial K}{\partial \lambda}\right|_{\lambda=\lambda_0} - F\left.\frac{\partial \widehat{\delta(\lambda)}^2}{\partial \lambda}\right|_{\lambda=\lambda_0}\right] \quad (24)$$

An achromatic critically-coupled design whose coupler length is $L\sim(2m\pm1)L_\pi(\lambda_0)/2$ simultaneously verifies equations (18), (22), (23) and presents an achromatic power-coupling efficiency as the evaluation of equation (24) shows that:

$$\left.\frac{\partial F(\lambda)}{\partial \lambda}\right|_{\lambda=\lambda_0} = 0 \quad (25)$$

With increasing resonator loss value and spectral dependence, the critical coupling conditions will shift away from the above-described limit cases ($L\sim mL_\pi(\lambda_0)$ or $L\sim(2m\pm1)L_\pi(\lambda_0)/2$), thereby the achromatic designs will result from a tailored interplay between the cavity loss wavelength dependence and the spectral evolutions of the coupler beat-length and power-transfer coefficient. Nevertheless, as it will be illustrated hereafter, the above scenarii constitute effective guidelines to design systems with the desirable achromatic critically-coupled behaviour.

3. NUMERICAL CASE STUDY

A. General considerations

At this stage, it is worth emphasizing that the model presented above, from which the two sets of favorable coupling conditions to obtain achromatic critically-coupled resonators were derived, is relatively generic. Indeed, the only assumption made is that the coupling between the resonator and the access waveguides occurs over an extended length of parallel waveguides and it can therefore be used to describe the spectral response of a variety of practical implementations including stadium resonators laterally coupled to their straight access waveguide [9], microdisk or microring resonators laterally (pulley-)coupled to curved waveguides [10], or WGM resonators that are vertically-coupled to their access waveguides [11]-[14]. The remainder of the article is devoted to a realistic numerical assessment of the benefits brought by such designs on a representative Si_3N_4/SiO_2 racetrack resonator system. In this study, the resonator is taken to be vertically-coupled to its access waveguide as this coupling scheme inherently offers the greatest engineering flexibility. Indeed, although not exploited in full hereafter, one could, in principle, vary the constitutive materials of each of the waveguides, change the waveguide cross-sections in two dimensions and also choose the relative vertical and lateral positions of the resonator with respect to the access waveguide to tailor the spectral characteristics of the system.

The numerical study is carried out with a nonlinear application of these systems in mind therefore the results will be presented in terms of their normalized intra-cavity power, $P_{int,N}(\lambda)$ defined as $P_{int,N}(\lambda)=P_{int}(\lambda)/P_{max}(\lambda)$ where $P_{max}(\lambda)$ is the maximum achievable intra-cavity power at the considered wavelength whose expression is:

$$P_{max}(\lambda) = [a(\lambda)^2(1-a(\lambda)^2)P_i(\lambda)]/[(1-a(\lambda)^2)^2] \quad (26)$$

As highlighted in the introduction, the objective of the paper is to design waveguide-coupled resonators whose critical coupling condition is met over the widest-possible wavelength range. To quantify this critical-coupling bandwidth, the selected criteria is taken to be the spectral range over which $P_{int,N}$>80%. The latter definition was selected as it can be applied to any system and tuned by adjustment of the limiting boundary value depending on the desired constraint on the critical coupling. We also note that the second order wavelength derivative of the merit function f could be considered as an alternative metric except that this parameter would only be meaningful for achromatic critically-coupled systems (i.e. systems already verifying equation (12a) or (13)).

B. Resonator design and characteristics

The system geometry under investigation is presented on Fig. 1 and 3. It consists of a 200-π-µm-perimeter rectangular resonator with 50-µm-radius rounded corners lying above its access waveguide. The resonator waveguide cross-section (see Fig. 3.a. and Fig. 5) is the same in the straight and bent sections and is taken to be 1250-nm-wide and 500-nm-high throughout this paper. This selection was based on bi-dimensional effective index calculations including material dispersion from references [15][16]. In this case, the resonator presents a near zero of averaged dispersion at a wavelength at 1550 nm and sustains single transverse TE-polarized guided mode propagation over a spectral region slightly larger than the 1500-2200nm wavelength range used to display the results. The particular shape of the resonator was chosen as a practical way to implement a fixed-loss resonator with variable coupling length. This is achieved by varying the distribution of the set 100-π-µm length between the four straight sections of the resonator (see Fig. 3). The coupling region is minimum when it reduces to the overlapping region between the curved portion of the resonator and the access waveguide (see lower diagram of Fig. 3a).

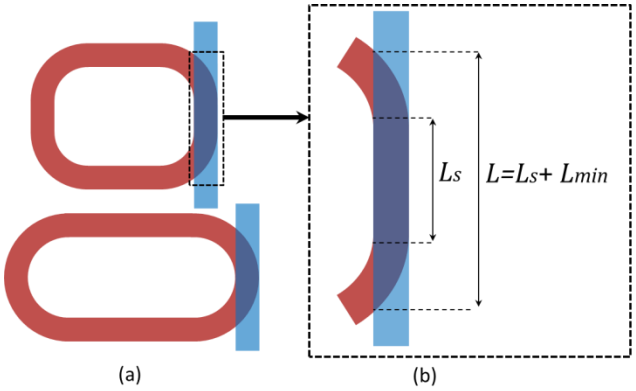

Fig. 3. Geometry of the vertically-coupled racetrack resonators under study showing (a) the resonator deformation permitting a variation of the coupling length while keeping constant the resonator loss and (b) a close-up view of the effective coupling length.

According to the experimentally-validated models of references [11]–[13], vertically-coupled WGM resonators with single transverse mode waveguides can be efficiently modelled using CMT considering the coupling region as being made of two parallel one-dimensional slab waveguides whose length, L, depends on the waveguides dimensions and positions. Following simple geometric considerations [17], for center-aligned waveguides as assumed here,

$$L = L_s + L_{min} = L_s + 2\sqrt{\frac{w_g+w_{res}}{2}\left(2R - \frac{w_g+w_{res}}{2}\right)} \qquad (27)$$

where R is the resonator external radius, w_{res} and w_g are respectively the resonator and access-waveguide widths and L_s is the length of the straight section of the resonator lying above the access waveguide. L_{min} is the minimum coupling length and occurs when the overlapping region is restricted to the overlap between the curved portion of the resonator and the access waveguide (see lower diagram of Fig. 3a). As an integral part of the above-mentioned approximation, the complete set of mode overlap coefficients is calculated by the one-dimensional numerical integration along the vertical axis of the TE-polarized guided mode profiles of the constitutive (resonator and access) decomposition waveguides defined according to the criterion detailed in [17]. The accuracy of this approximation will obviously improve as the considered waveguides resemble slab-like waveguides i.e. are horizontally elongated.

Given the large bending radius considered, the resonator loss is assumed to be dominated by the scattering losses occurring at the sidewalls of the waveguides. To estimate the resonator loss spectral dependence, we have implemented an analytical expansion of the widely accepted and reasonably accurate Payne-Lacey scattering loss model [18][19]. The results using a RMS roughness $\sigma_r = 3nm$ are shown in Fig. 4. At a wavelength of 1550 nm, the propagation loss coefficient is calculated to be ρ=0.297 cm^{-1}, corresponding to an intrinsic Q-factor Q_i=478 10^3, to a=99.01%, values consistent with experimentally reported devices [2]. The spectral loss dependence is also found to be relatively weak as $\partial a(\lambda)^2/\partial\lambda$=2.6 10^{-6}/nm. It is worth pointing out here, that since the resonator loss characteristics are kept unchanged in the remainder of this study, the maximal intra-cavity power value achieved at critical coupling in the coupled systems under investigation is independent of the coupler internal design (i.e. independent of whether the coupler constitutive waveguides are (quasi-)phase matched or phase mismatched).

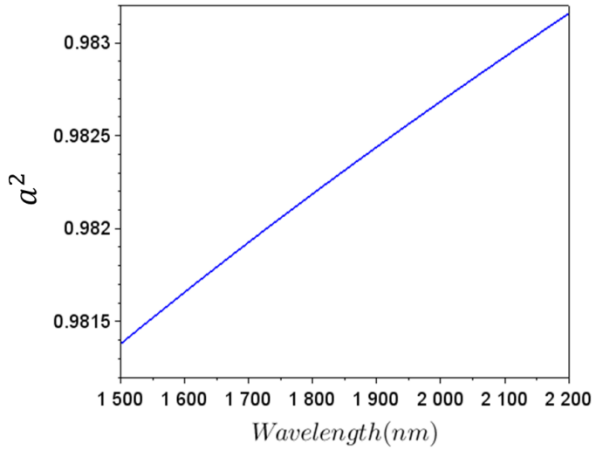

Fig. 4. Calculated spectral characteristics of the resonator's intensity inner circulation factor a^2.

C. Reference (quasi-)phase-matched scenario

We begin the study of the coupled resonator systems with a configuration considered as the reference or (quasi-)phase-matched (QPM) case where by, as conventionally done, the access waveguide (1200-nm-) width and (452-nm-) height are chosen in such way that the supported mode presents the same effective index as the mode propagating in the resonator resulting in $\widehat{\delta(\lambda)} = 0$. The latter condition is only met at a single wavelength (1550 nm) since the surroundings of the two waveguides differ (see Fig. 5), and thereby this scenario is strictly-speaking only a quasi-phase-matched situation ($\Delta n_{eff}(\lambda)$<4.8 10^{-3} over the spectral range of interest). Nevertheless, for a 200.00-nm separation distance, the ratio $\widehat{\delta(\lambda_0)}^2/K(\lambda_0) = 4.06\ 10^{-6}$ shows that the coupler characteristics are clearly dominated by the coupling term K and the system can then be considered as phase-matched. This waveguide was also checked to be singlemode over the spectral region of interest.

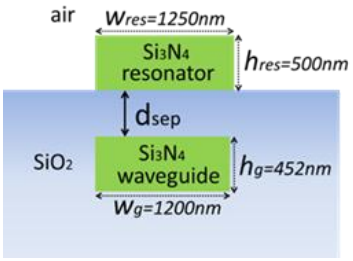

Fig. 5. Cross-section of the considered (quasi-)phase-matched racetrack resonator

Fig. 6 shows the evolution of the intra-cavity power spectrum as a function of the length of the coupler, starting from a value close to its minimum value, L_{min}~22 µm (see equation (27)), and for a vertical separation between the resonator and the access waveguide, d_{sep}, set to 200.00 nm. The analysis of the plotted map at various fixed wavelengths shows that the critical coupling conditions (identifiable as the bright areas on Fig. 6) occur for several coupler lengths with a periodicity of L_π (materialized as the black regions) as described by equation (13). Defining the fundamental coupling order as the first critical coupling order, $m_{min}{}^{\pm}$, such that $L_{cc}(\lambda, m_{min}{}^{\pm}) > L_{min}$ (= 22 µm), one can determine that $m_{min}{}^{-}$=2, observing that $L_\pi(\lambda_0$=1550 nm, d_{sep}=200.00 nm)= 12.18 µm. As evidenced by the strong spectral curvature of the bright areas on Fig. 6, the critical coupling conditions are clearly strongly chromatic. This is always the case for devices with (quasi-)phase-matched waveguides as the achromatic condition of equation (15) can not be met $\left(\text{as } \partial K/\partial\lambda|_{\lambda=\lambda_0} > 0\right)$. Indeed, the observed spectral evolution is a direct consequence of the fact that, according to equation (5), when the waveguide phase-mismatch is negligible, L_π is entirely governed by the evolution of the modal overlap coefficients $(\kappa_a(\lambda), \kappa_b(\lambda))$ and that these parameters monotonically increase with the weakening of modal confinement at long wavelengths. Furthermore, as shown in Fig. 6 by the increasingly horizontally tilted bright lines as L increases, at a set separation between the resonator and its access waveguide, solutions with larger critical coupling order $m^{\pm}$ present worse chromatic dependence. This can also be inferred from equation (13) where the coupling order is shown to exacerbate the influence of the spectral curvature of L_π.

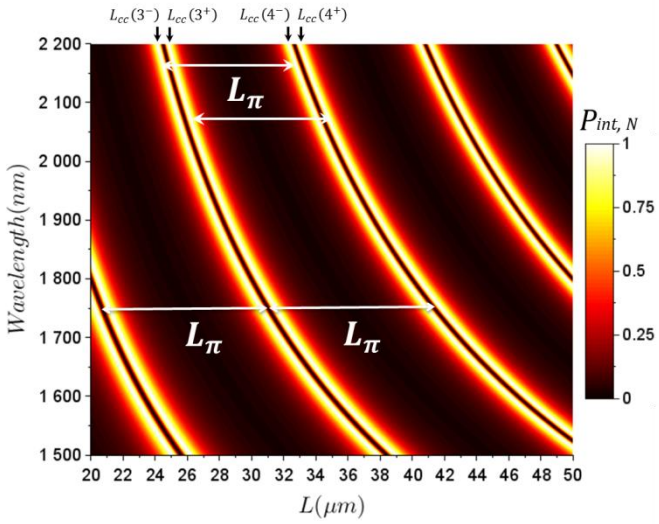

Fig. 6. Normalized intra-cavity power map for a separation distance d_{sep}=200 nm for a system with (quasi-)phase-matched resonator and access waveguides.

In order to better understand the behaviour shown in Fig. 6, and in the following intracavity power spectral maps (Fig. 10 and 11), one should refer to Fig. 2 recognizing that it corresponds to a cross section of these two-dimensional maps at a fixed wavelength. The bright regions in the spectral maps thus correspond to the intersection points around integer multiples of L_π and occur periodically along the coupler length L because of the $|t(L)|^2$ oscillatory power transfer pattern.

In the remainder of the paper, we will therefore limit our study to the fundamental order cases. The spectral response obtained for $\boldsymbol{m_{min}}^{\pm}$, shown in red on Fig. 7, is therefore the least wavelength-dependent, and its achromatic bandwidth is found to be 23 nm wide. It is worth pointing out at this point that, by increasing the separation between the resonator and the access waveguides i.e. by increasing $\boldsymbol{L_\pi(\lambda_0)}$, a given coupling length (L_{min} for instance) might correspond to several critical coupling orders. However, numerical tests (not shown here) reveal that the spectral dependence of L_π at small separation distance is weaker and compensates for the curvature enhancement induced by the higher critical coupling order and thereby results in almost identical achromatic bandwidths.

D. Phase-mismatched cases

Having shown that (quasi-)phase-matched structures are not suitable to obtain achromatic critically-coupled systems, the study is furthered by investigating the opportunities offered by the use of phase-mismatched (PMM) structures.

1. Achromatic beat-length coupler scenario

To that extent, the access waveguide is modified while keeping the resonator design identical. The access waveguide cross-section was selected to obtain an achromatic beat-length system, i.e. chosen such that it meets equation (19) (or equivalently (21)). Since $K(\lambda)$ exhibits a slowly increasing spectral variation, the mismatch is taken to show the opposite wavelength dependence (see Fig. 9) over the widest spectral range for an appropriately set separation between the resonator and the access waveguide, d_{sep}. As shown in Fig. 8, the resulting access waveguide cross-section is 1700-nm-wide and 250-nm-thick and the separation between the resonator and access waveguide is 293.75 nm. This geometry only supports TE-polarised singlemode propagation over the 1500-2200-nm spectral range and, according to equation (27), the associated minimum coupling length is L_{min}~24 µm.

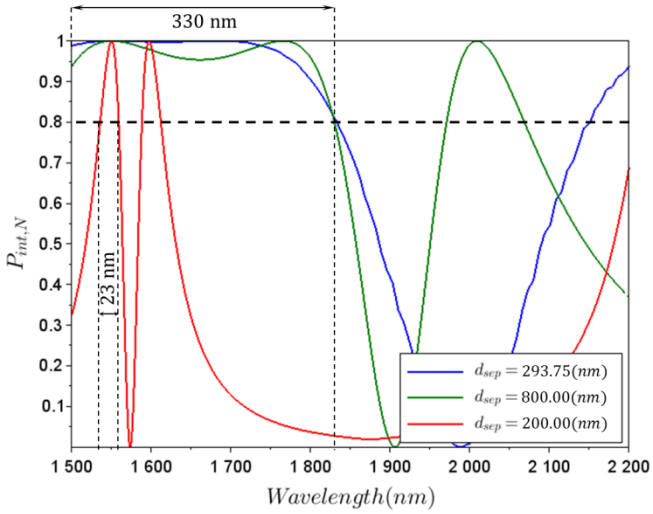

Fig. 7. Evolution of the normalized intra-cavity power $P_{int,N}$ as a function of wavelength in (a) the PM case (red curve) with d_{sep}=200.00 nm and the PMM case at (b) optimal waveguide separation distance for scenario 1 d_{sep} = 293.75 nm (blue curve), and (c) optimimal separation for scenario 2, at the cut-off separation distance d_{sep} = 800.00nm (green curve).

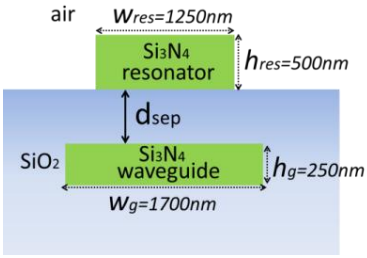

Fig. 8. Cross-section of the phase-mismatched racetrack resonator.

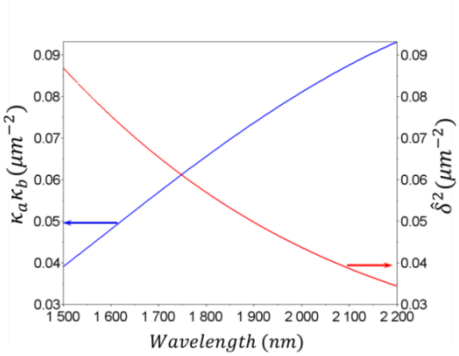

Fig. 9. Evolution of $\kappa_a\kappa_b(\lambda)$ and $\hat{\delta}^2(\lambda)$ in the PMM case at the optimal waveguide vertical separation distance d_{sep}=293.75 nm.

The analysis of this PMM scenario begins by representing in Fig. 10 the dependence of normalized intracavity power spectrum as a function of the coupler length for the separation of 293.75 nm. The interpretation of this map is similar to the PM case (Fig. 6) except for the fact that, here, the critical coupling conditions exhibit insignificant spectral dependence (since the bright regions are almost vertical). In these circumstances, the system achromatic behaviour results from the coupler beat-length achromatic characteristics as attested by the evolutions of $\kappa_a\kappa_b(\lambda)$ and $\hat{\delta}^2(\lambda)$ plotted in Fig. 9 and shown in Fig. 12. Selecting the fundamental coupling order (m_{min}^{-}=3 deduced from L_{cc}=24.4 µm ; L_π= 8.34µm; and leading to x_0=0.074 L_π), the device response, displayed as the blue curve in Fig. 7, is shown to have an achromatic bandwidth greater than 330 nm.

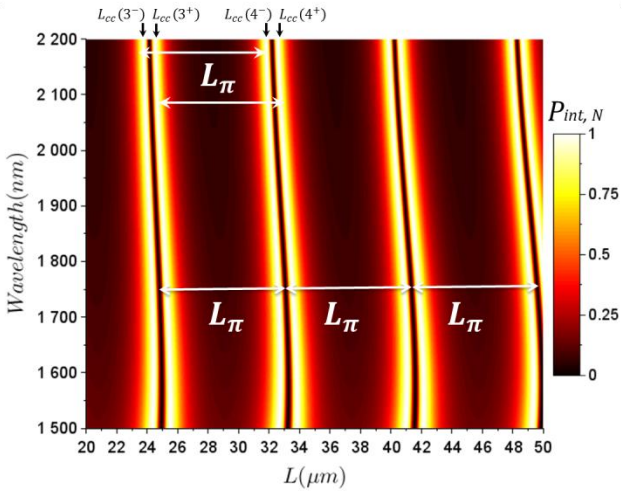

Fig. 10. Evolution of the normalized intra-cavity power as a function of coupler length and wavelength, in the PMM case for the optimal waveguide separation distance (dsep= 293.75nm). Here, the coupling orders correspond to m=3,4,5.

2. Achromatic power-transfer coupler scenario

As suggested in the theoretical section of the paper, moving from the achromatic beat-length scenario to the achromatic power-transfer case can be achieved by tuning the amplitude of the power transfer oscillations, *F*, such that the minimum of the $|t|^2$ spatial oscillations becomes tangent to a^2 (see Fig. 2), leaving unchanged the resonator and access waveguide cross-sections. Since *F* is a decreasing function of d_{sep} (see equation (10)), this occurs when d_{sep} is increased to 800.00 nm, thickness beyond which equation (12a) no longer has solutions as the system operates in the deep under-coupling regime. The general behaviour of the system is clearly modified by this increase in the separation between the resonator and the access waveguides from 293.75 nm (Fig. 10) to 800.00 nm (Fig. 11). In the 800.00-nm-separation case, spectrally-wide critical coupling regions can still be found (bright areas at L~27 µm, 38 µm) in spite of the coupler beat-length presenting a strong wavelength dependence (oblique black regions). For a wavelength of 1550 nm, the points corresponding to the critical coupling condition can be observed to be mid-way between the curves associated to the multiple orders of L_π (black region) as ruled by equation (13).

The numerical investigation of this scenario reveals that equation (25) is not strictly satisfied : as shown in Fig. 12, the derivative $\frac{\partial F(\lambda)}{\partial\lambda}\Big|_{\lambda=\lambda_0}$ is non-zero but exhibits its smallest value over the d_{sep} range of interest at the cut-off separation distance d_{sep} =800.00 nm (whereas $\frac{\partial L_\pi}{\partial\lambda}\Big|_{\lambda=\lambda_0}$ is strictly zero for d_{sep} = 293,75 nm). The spectrally-wide critical coupling regions of Fig. 11 stem from this minimum of chromaticity for F. For L=27.94 µm, given that L_π=11.17 µm, the fundamental coupling order can be found to be $m_{min}^{\pm}$=3. The corresponding device response is shown in green in Fig. 7 and demonstrates a quasi- achromatic bandwidth exceeding 330-nm.

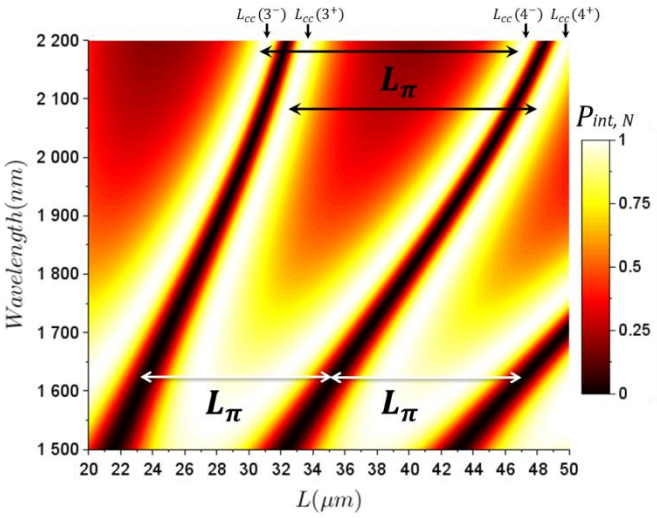

Fig. 11. Evolution of the normalized intra-cavity power spectrum as a function of the coupler length in the PMM case for a separation between the resonator and the access waveguide of 800.00 nm.

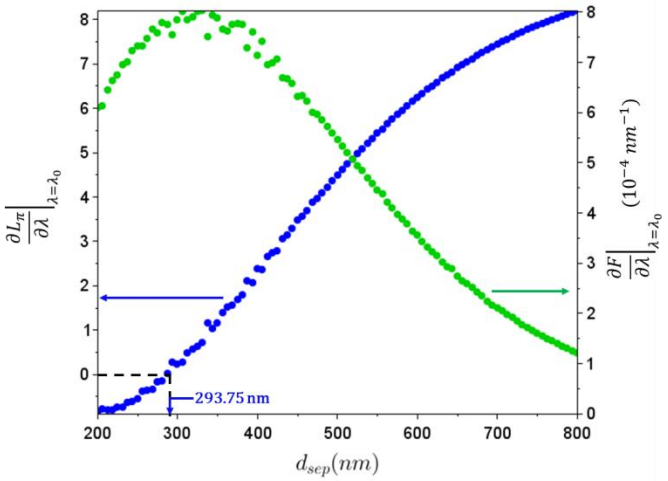

Fig. 12. Evolution of the chromaticity of the coupler beat-length L_π (left axis, blue dots) and of the power coupling efficiency *F* (right axis, green dots) as a function of the waveguide vertical separation distance d_{sep}.

3. Stability and tolerance study of the achromatic critically-coupled designs

Having established two experimentally-viable designs to obtain achromatic or quasi-achromatic critically-coupled Si_3N_4/SiO_2 racetrack resonators, we now investigate the stability and parameter tolerance of the latter designs. To begin with, the evolution of the normalized intracavity power spectrum as a function of the separation between the resonator and the access waveguide for a device whose coupler length is taken to be the critical-coupling length of order $m_{min}^{\pm}=3^-$ is represented in Fig. 13 (a). The associated variation of the selected critical coupling length is shown in Fig. 13 (b). The plotted results (Fig. 13 (a)) prove that wideband critical coupling only occurs at two specific separations, 293.75 nm and 800.00 nm, corresponding respectively to the achromatic-L_π scenario and achromatic-F case as highlighted above. The adjustment of d_{sep}~300 nm essentially tunes the center wavelength of the achromatic critically-coupled regime with a minor change in the achromatic bandwidth. We note that both achromatic critically-coupled designs require the separation thickness to be controlled with a rather stringent but still technologically-feasible 10-nm precision to keep the critical-coupling bandwidth larger than 80% of its optimum value. This should be compared to the QPM case where the critical-coupling bandwidth of 23nm can be maintained within a d_{sep} variation of 100-nm. Although the latter tolerance value may suggest that the QPM structures are more forgiving, Fig. 13 (a) also highlights that, in the studied PMM case, the critical-coupling bandwidth is at least two times larger than the QPM one over the entire 600-nm d_{sep} span.

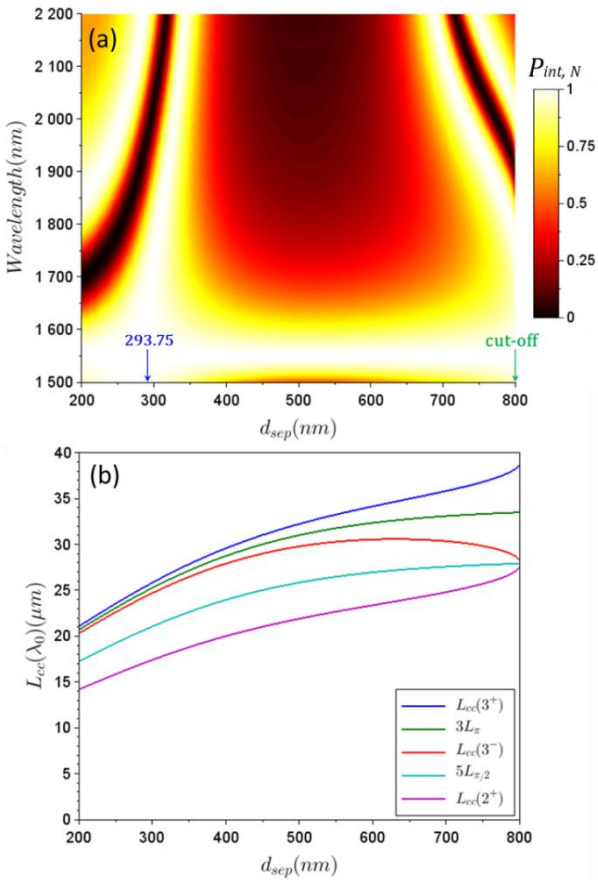

Fig. 13. (a) Evolution of the normalized intra-cavity power as a function of the waveguide separation distance and wavelength, in the PMM case for the critical coupling order m=3+. (b) Evolution of selected critical coupling lengths and coupler characteristic lengths as a function of the waveguide separation distance.

We continue this stability analysis by studying how the chosen phase-mismatch between the resonator and access waveguides influences the remainder of the design and how this parameter impact on the achievable performance. In the achromatic L_π situation, as shown in Fig. 14 (a), when the access waveguide thickness h_g is decreased, the phase mismatch increases (from Δn_{eff}= 3.13 10^{-2} to 14.5 10^{-2}), and the spectral bandwidth over which L_π can be made wavelength-insensitive expands. Therefore the system achromatic bandwidth increases. The maximum bandwidth limit is indirectly set by the fact the resonator-access waveguide separation distance needs to be consequently linearly reduced, as highlighted by the blue curve of Fig.14 (b) and by the singlemode cut-off wavelength. In the achromatic-F case (see Fig. 15), choosing a reduced phase mismatch (i.e. increasing the access waveguide thickness h_g) entails to use a larger resonator-to-access-waveguide separation as highlited by the blue curve of Fig. 15 (b) and reduces the quasi-achromatic critical coupling bandwith. Here again, the limiting factors are the resonator to access waveguide separation and associated critical-coupling length.

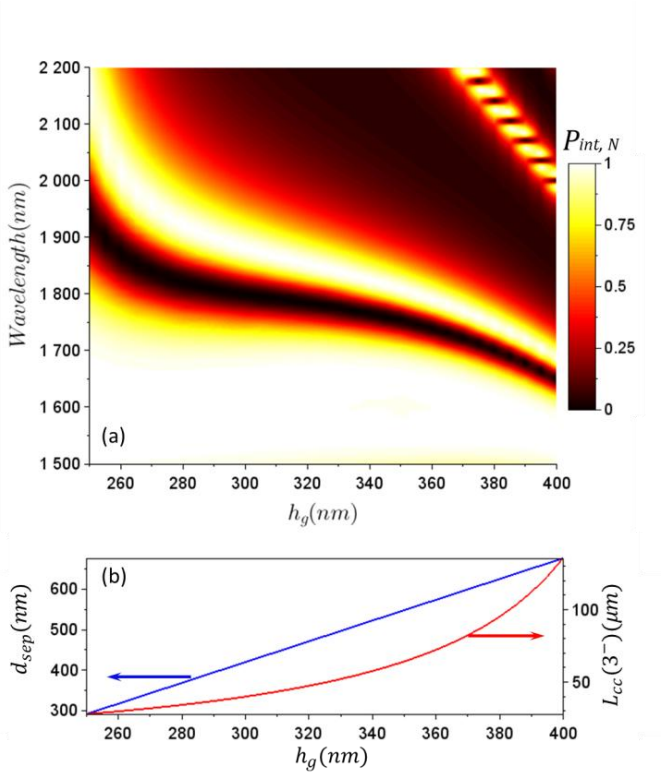

Fig. 14. (a) : evolution of the normalised intracavity power spectrum as a function of the access waveguide thickness h_g (resulting in a varying $\hat{\delta}^2$) for the achromatic-L_π scenario. (b) : evolution of the separation distance at which the achromatic-L_π scenario occurs (blue curve) and of the correspopnding critical coupling length (red curve) as a function of the access waveguide thickness h_g.

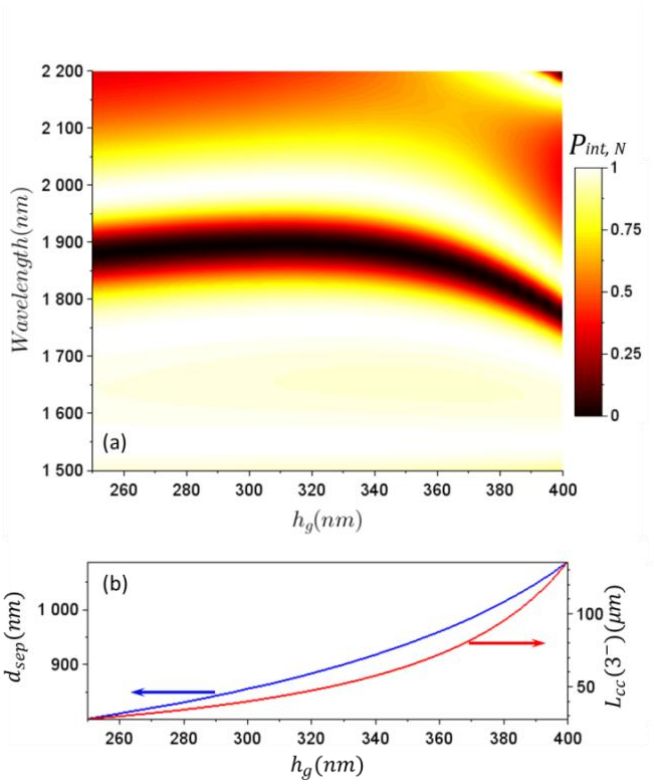

Fig. 15. (a) Evolution of normalised intracavity power spectrum as a function of the access waveguide thickness h_g (resulting in a varying δ^2) for the achromatic-*F* scenario. (b) : evolution of the separation distance at which the achromatic-*F* scenario occurs (blue curve) and of the corresponding critical coupling length (red curve) as a function of the access waveguide thickness h_g.

4. CONCLUSIONS

In this work, we have theoretically established two sets of favorable conditions to obtain whispering-gallery-mode resonators which are critically-coupled over a wide spectral range to their access waveguide. Typically, the above-mentioned achromatic designs involved using a resonator and an access waveguide with mismatched propagation constants and setup in a way to establish a coupling region exhibiting either an achromatic beat-length or an achromatic power-transfer coefficient. As this theoretical derivation was performed using a generic model based on the universal description of the system characteristics and a coupled-mode treatment of the parallel-waveguide coupling section, it could be applied to a variety of practical embodiments. Subsequently, a parametric numerical study of vertically-coupled Si_3N_4/SiO_2 racetrack resonators showed that the achromatic designs were practically implementable and permitted the achromatic critical-coupling bandwidth to be broadened by one order of magnitude in comparison to a critically-coupled system with (quasi-)phase-matched waveguides.

Funding. French space agency CNES (R&T contract : « frequency combs on a chip »); Délégation Générale de l'Armement and Centre National d'Etudes Spatiales (C. Arlotti's PhD studentship).

REFERENCES

[1] A. B. Matsko and V. S. Ilchenko, "Optical resonators with whispering gallery modes I: basics," *IEEE J Sel Top Quantum Electron*, vol. 12, no. 1, pp. 3–14, 2006.

[2] M. A. Foster, J. S. Levy, O. Kuzucu, K. Saha, M. Lipson, and A. L. Gaeta, "Silicon-based monolithic optical frequency comb source," *Opt. Express*, vol. 19, no. 15, p. 14233, Jul. 2011.

[3] J. Ward and O. Benson, "WGM microresonators: sensing, lasing and fundamental optics with microspheres," *Laser Photonics Rev.*, vol. 5, no. 4, pp. 553–570, Jul. 2011.

[4] Y. Sun and X. Fan, "Optical ring resonators for biochemical and chemical sensing," *Anal. Bioanal. Chem.*, vol. 399, no. 1, pp. 205–211, Jan. 2011.

[5] T. J. Kippenberg, S. M. Spillane, and K. J. Vahala, "Modal coupling in traveling-wave resonators," *Opt. Lett.*, vol. 27, no. 19, p. 1669, Oct. 2002.

[6] A. Yariv, "Universal relations for coupling of optical power between microresonators and dielectric waveguides," *Electron. Lett.*, vol. 36, no. 4, pp. 321–322, 2000.

[7] S. Chandran, R. K. Gupta, and B. K. Das, "Dispersion Enhanced Critically Coupled Ring Resonator for Wide Range Refractive Index Sensing," *IEEE J. Sel. Top. Quantum Electron.*, vol. 23, no. 2, pp. 424–432, Mar. 2017.

[8] K. Okamoto, *Fundamentals of optical waveguides*, 2nd ed. Amsterdam ; Boston: Elsevier, 2006.

[9] G. Griffel, J. H. Abeles, R. J. Menna, A. M. Braun, J. C. Connolly, and M. King, "Low-threshold InGaAsP ring lasers fabricated using bi-level dry etching," *IEEE Photonics Technol. Lett.*, vol. 12, no. 2, pp. 146–148, Feb. 2000.

[10] E. Shah Hosseini, S. Yegnanarayanan, A. H. Atabaki, M. Soltani, and A. Adibi, "Systematic design and fabrication of high-Q single-mode pulley-coupled planar silicon nitride microdisk resonators at visible wavelengths," *Opt. Express*, vol. 18, no. 3, p. 2127, Feb. 2010.

[11] M. Ghulinyan *et al.*, "Oscillatory Vertical Coupling between a Whispering-Gallery Resonator and a Bus Waveguide," *Phys. Rev. Lett.*, vol. 110, no. 16, p. 163901, Apr. 2013.

[12] F. Mandorlo, P. Rojo Romeo, X. Letartre, R. Orobtchouk, and P. Viktorovitch, "Compact modulated and tunable microdisk laser using vertical coupling and a feedback loop," *Opt. Express*, vol. 18, no. 19, pp. 19612–19625, 2010.

[13] F. Turri, F. Ramiro-Manzano, I. Carusotto, M. Ghulinyan, G. Pucker, and L. Pavesi, "Wavelength Dependence of a Vertically Coupled Resonator-Waveguide System," *J. Light. Technol.*, vol. 34, no. 23, pp. 5385–5390, Dec. 2016.

[14] S. Calvez *et al.*, "Vertically Coupled Microdisk Resonators Using AlGaAs/AlOx Technology," *IEEE Photonics Technol. Lett.*, vol. 27, no. 9, pp. 982–985, May 2015.

[15] M. Bass, V. N. Mahajan, and Optical Society of America, Eds., *Handbook of optics*, 3rd ed. New York: McGraw-Hill, 2010.

[16] T. Bååk, "Silicon oxynitride; a material for GRIN optics," *Appl. Opt.*, vol. 21, no. 6, p. 1069, Mar. 1982.

[17] C. Arlotti, G. Almuneau, O. Gauthier-Lafaye, and S. Calvez, "Coupled mode analysis of micro-disk resonators with an asymmetric-index-profile coupling region," in *proc. of SPIE*, San Francisco, California, USA, 2017, vol. 10090, p. 100901D.

[18] F. P. Payne and J. P. R. Lacey, "A theoretical analysis of scattering loss from planar optical waveguides," *Opt. Quantum Electron.*, vol. 26, no. 10, pp. 977–986, Oct. 1994.

[19] L. J. McKnight, M. D. Dawson, and S. Calvez, "Diamond Raman Waveguide Lasers: Completely Analytical Design Optimization Incorporating Scattering Losses," *IEEE J. Quantum Electron.*, vol. 47, no. 8, pp. 1069–1077, Aug. 2011.